

# Neural Propagation of Beliefs

M.J. Barber\*    J.W. Clark†    C.H. Anderson‡

December 2, 2024

## Abstract

It has been proposed that populations of neurons process information in terms of probability density functions (PDFs) of analog variables. Such analog variables range, for example, from target luminance and depth on the sensory interface to eye position and joint angles on the motor output side. The requirement that analog variables must be processed leads inevitably to a probabilistic description, while the limited precision and lifetime of the neuronal processing units leads naturally to a population representation of information. By encoding the probability density over the relevant analog variables, the neural ensemble can in principle answer any meaningful question about these analog variables, by implementing the Bayesian rules for information propagation. We show how a time-dependent probability density  $\rho(x; t)$  over variable  $x$ , residing in a specified function space of dimension  $D$ , may be decoded from the neuronal activities in a population as a linear combination of certain decoding functions  $\phi_i(x)$ , with coefficients given by the  $N$  firing rates  $a_i(t)$  (generally with  $D \ll N$ ). We show how the neuronal encoding process may be described by projecting a set of complementary encoding functions  $\hat{\phi}_i(x)$  on the probability density  $\rho(x; t)$ , and passing the result through a rectifying nonlinear activation function. We show how both encoders  $\hat{\phi}_i(x)$  and decoders  $\phi_i(x)$  may be determined by minimizing cost functions that quantify the inaccuracy of the representation. Expressing a given computation in terms of manipulation and transformation of probabilities, we show how this representation leads to a neural circuit that can carry out the required computation within a consistent Bayesian framework, with explicit construction of the synaptic weights in terms of encoders,

---

\*Institut für Theoretische Physik, Universität zu Köln, D-50937 Köln, Germany

†Department of Physics, Washington University, Saint Louis, MO 63130

‡Department of Anatomy and Neurobiology, Washington University School of Medicine, Saint Louis, MO 63110

decoders, conditional probabilities, and priors. Finally, aided by an intermediate representation of the probability density based on orthogonal functions spanning the underlying  $D$ -dimensional function space, we show how such neural circuits may be generated from Bayesian belief networks. The ideas and the formalism of this PDF approach are illustrated and tested in several simple examples, including design of a communication channel, estimation of the velocity of a moving object, and solution of a problem in which model-driven top-down information flow influences the processing of bottom-up sensory input.

## 1 Introduction

### 1.1 Fundamental Hypothesis

The anatomy of the cerebral cortex shows strong feedforward, feedback, and lateral interconnections that are absent in cerebellar, sensory, or motor output circuits. Distinct cortical areas associated with various aspects of higher cognitive function have been described based on anatomical, physiological, and behavioral information. A possible explanation (Van Essen *et al.*, 1992) for this anatomical structure is that the cortical areas support a modular approach to solving complex problems, with different areas optimized for different subtasks in neural information processing. For such a modular strategy to be effective, it is essential that coordinated and efficient routing of information is maintained between modules, necessitating extensive connections between cortical areas.

It has been hypothesized (Anderson, 1994) that circuits of cortical neurons perform statistical inference, and, in particular, that they encode and process information about analog variables in the form of probability density functions (PDFs). This PDF hypothesis provides a unified framework for understanding diverse observations from experimental neurobiology, constructing neural network models, and generating insights into how neurons can implement a rich collection of information-processing functions.

Importantly, if neural populations encode the joint probability distribution over the variables of interest, then such neural networks are able to answer any probabilistic question about those variables. With this in mind, it is sensible to extend the PDF hypothesis by exploring methods for embedding joint probabilities into neural networks. This will enable us to construct neural networks that pool multiple sources of evidence, such as sensory inputs and any evolutionarily-determined priors on the joint distribution. In particular, we will focus on developing neural networks that use “bottom-up” sensory inputs to build

an internal model of the data, which in turn uses “top-down” signals to impose global regularities on the sensory data. We will see that distinct feedforward, feedback, and lateral connections arise naturally in the resulting neural networks.

In developing these neural networks, we will make use of Bayesian belief networks (Pearl, 1988; Smyth *et al.*, 1997). Bayesian belief networks are graphical representations of probabilistic models and provide a convenient means for organizing the relations between the random variables of a given model. The resulting neural networks will have several properties of Bayesian belief networks, as well as more typical neural network properties, so we will term them *neural belief networks*.

## 1.2 Experimental and Theoretical Motivation

The PDF hypothesis derives from two major themes. The first theme stems from attempts to determine how information is represented by neural systems by understanding how neural activity correlates to external cues or actions (such as sensory stimuli or motor response). Our understanding of neural encoding can be tested by inferring sensory input or motor output from a set of neural activities, and comparing the estimate thus obtained to the external cue or action.

To decode the response from a population of neurons requires procedures to infer information from individual spike trains, as well as procedures to combine these results into an aggregate estimate. An optimal method for decoding information from individual neural spike trains has been developed (Bialek *et al.*, 1991, 1992; Rieke *et al.*, 1997) and applied to movement-sensitive neurons in the blowfly (Rieke *et al.*, 1997) and to other systems (Theunissen *et al.*, 1996). This method consists of utilizing a linear filter to extract the maximum possible information from each spike (typically a few bits; see Rieke *et al.*, 1997), as measured by the ability to reconstruct the stimulus from the spike train. In these studies, the linear filter determines a firing rate from the spike trains; this firing rate contains most of the information, with additional information possibly encoded in other aspects of the activity patterns. (For the development of the neural belief networks, we will assume that the firing rates capture the essential behavior of neural systems, and will not explicitly consider spike trains.)

It is in fact quite surprising that a linear filter is effective at decoding a neural spike train, since the spike generation process is highly nonlinear (Abbott and Kepler, 1990). Further, the linear decoding process quantifies the precision of the neurons, raising the question of how processing elements with such limited precision (about 3 bits) and short memory time (about 10 ms) can be organized to build powerful computational circuits. This question is of course still open. It is clear that the organization of neuronal circuits is very different from the

organization of digital computers. Digital computers utilize carefully-organized representations of numbers to maximize information capacity, while neuronal circuits are highly redundant systems that trade off some representational ability in favor of robustness against loss of processing elements.

Methods for decoding information from the firing rates of populations of neurons were pioneered by Georgopoulos and collaborators. They showed that a “population vector” derived from the firing rates of a population of cortical neurons can be used to predict the intended arm movements of monkeys (Georgopoulos *et al.*, 1986; Schwartz, 1993). This vector estimate of direction,  $\mathbf{V}_{\text{est}}$ , is obtained from the neural firing rates  $a_i$  by

$$\mathbf{V}_{\text{est}} = \sum_{i=1}^N a_i \mathbf{C}_i \quad (1)$$

where the preferred direction vectors,  $\mathbf{C}_i$ , indicate the direction at which neuron  $i$  has its maximal firing response. The population vector approach has been refined and extended by several authors; in particular, Salinas and Abbott (1994) provide an excellent discussion of several such refinements, as well as introducing their own. The emphasis in such studies has been the reconstruction of vector quantities from populations of neural responses by a process that in several cases appears to be computation of an expectation value from an implicit probability distribution.

The second theme leading to the PDF hypothesis stems from an analysis showing that the original Hopfield neural network implements, in effect, Bayesian inference on analog quantities in terms of PDFs (Anderson and Abrahams, 1987). While the role of PDFs in neural information processing is still being explored, there are a number of works worth noting. Zemel *et al.* (1998) investigated population coding of probability distributions, but with different representations than those we will consider here. Several extensions of this representation scheme have been developed (Zemel, 1999; Zemel and Dayan, 1999; Yang and Zemel, 2000) that feature information propagation between interacting neural populations. Further, a number of related models have been investigated. Of particular note is a dynamic routing model of directed attention (Anderson and Van Essen, 1987; Olshausen *et al.*, 1993,1995). Additionally, several “stochastic machines” (Haykin, 1999) have been formulated, including Boltzmann machines (Hinton and Sejnowski, 1986), sigmoid belief networks (Neal, 1992), and Helmholtz machines (Dayan and Hinton, 1996). Stochastic machines are built of stochastic neurons that reside in one of two possible states in a probabilistic manner; learning rules for stochastic machines in essence model the underlying probability distribution of a given

data set. These machines are unrealistic as models of biological neural networks, however.

These two themes are combined in the PDF hypothesis through the assertion that a physical variable  $x$  is described by a neural population at time  $t$  in terms of a PDF  $\rho(x; t)$ , rather than as a single-valued estimate  $x(t)$ . Such a PDF description has the significant advantage that it not only permits a single-valued estimate to be calculated, but also provides for a measure of the uncertainty of these estimates. For example, a specific value  $\xi$  at time  $t$  can be represented as the mean of a normal distribution over  $x$  with variance  $\sigma^2$

$$\rho(x; t) = N(x; \xi(t), \sigma^2(t)) \quad (2)$$

Clearly, this PDF allows  $\xi(t)$  to be known very precisely (small variance) or with a great deal of uncertainty (large variance).

More generally, we consider a PDF described at time  $t$  in terms of a set of  $D$  parameters  $\{A_\mu\}$ . Guided by the experimentally-observed linear decoding rules discussed above, we will take the PDFs to be represented by

$$\rho(x; t) \equiv \rho(x; \{A_\mu(t)\}) = \sum_{\mu=1}^D A_\mu(t) \Phi_\mu(x) \quad (3)$$

The basis functions  $\Phi_\mu(x)$  are orthonormal functions that define the PDFs that the neural circuit can represent, while the quantity  $D$  is seen to be the dimensionality of the space of PDFs which the neural circuit can represent. We describe  $x$  with  $\rho(x; \{A_\mu(t)\})$  rather than  $\rho(x | \{A_\mu(t)\})$  to distinguish between the assumed forms of models (equation 3) and relationships that exist amongst random variables (conditional probabilities).

The amplitudes  $A_\mu(t)$  of the representations defined by equation 3 cannot be interpreted as neuronal firing rates: the amplitudes can take on negative values and are more precise than neuronal firing rates. However, we can represent a PDF in terms of decoding functions  $\phi_i(x)$  and firing rates  $a_i(t)$  associated with  $N$  neurons, so that

$$\rho(x; t) = \sum_{i=1}^N a_i(t) \phi_i(x) \quad (4)$$

Unlike the basis functions  $\Phi_\mu(x)$ , the decoding functions  $\phi_i(x)$  form a highly redundant, overcomplete representation ( $N \gg D$ ) that is specialized for use with neurons of limited precision.

The abstract representation defined by equation 3 will underlie the representation in the neuron space defined by equation 4. This allows us to deal with the issue of how PDFs can be precisely implemented in

ensembles of neurons by focusing on the mapping between the underlying space and the space of neurons. Thus, neural belief networks can be developed in the theoretically-convenient abstract representation, and then be implemented in more realistic networks of low-precision model neurons. Following Zemel *et al.* (1998), we denote the set of physical variables as the *implicit space* and the measurable quantities as the *explicit space*. Extending their nomenclature, we denote the abstract space of equation 3 as the *underlying space*. The explicit space of neurons constitutes a physical implementation of the desired computations in the implicit space, requiring us to face the issues of noise and the highly nonlinear encoding properties of the neurons (see section 2). The underlying space serves as a useful bridge between these two other spaces.

It may be conceptually helpful to regard the variables or parameters  $A_\mu(t)$  as the activities of a set of  $D$  “metaneurons,” fictitious entities that reside and act in the underlying space. As already indicated, such metaneurons differ from real neurons in their abilities to function with high precision and to produce negative “firing rates”  $A_\mu(t)$ . Accordingly, they possess valuable properties that will facilitate formal representation and analysis.

## 2 Obtaining the Neuronal Representation

### 2.1 Multiple Levels of Representation

The fundamental assumption of the framework to be developed in this paper is that information about a physical variable  $x$  given a set of parameters  $\mathbf{A} = \{A_1, A_2, A_3, \dots\}$  at time  $t$  is represented by an ensemble of neurons as a PDF  $\rho(x; A_1(t), A_2(t), A_3(t), \dots)$ . For notational convenience, we will frequently abbreviate this quantity as  $\rho(x; t)$ . This PDF can be extracted from a set of neuronal firing rates  $\{a_i(t)\}$  using a set of decoding functions (or simply decoders)  $\phi_i(x)$ , according to

$$\rho(x; t) = \sum_i a_i(t) \phi_i(x) \quad (5)$$

A set of encoding functions (encoders)  $\hat{\phi}_i(x)$  is used to determine the firing rates from an assumed PDF by means of

$$a_i(t) = f \left( \int \hat{\phi}_i(x) \rho(x; t) dx \right) \quad (6)$$

where a nonlinear activation function  $f()$  is introduced to prevent negative firing rates. These rules permit us to map information between the implicit and explicit spaces. The decoding rule (equation 5) must be viewed as only returning an approximation to the PDF, however:

functions that are not strictly positive semidefinite can be decoded from such a rule.

We can also represent the PDF using a complete orthonormal basis  $\{\Phi_\mu(x)\}$  for the space spanned by the decoders

$$\rho(x;t) \equiv \rho(x; \{A_\mu(t)\}) = \sum_{\mu=1}^D A_\mu(t) \Phi_\mu(x) \quad (7)$$

Further, we can represent the decoding functions in terms of this basis

$$\phi_i(x) = \sum_{\nu=1}^D \kappa_{\nu i} \Phi_\nu(x) \quad (8)$$

where the  $\kappa_{\nu i}$  are coupling constants to be determined.

Since we now have an orthonormal basis, the coefficients  $A_\mu$  in equation 7 are simply determined in the familiar way

$$A_\mu(t) = \int \Phi_\mu(x) \rho(x;t) dx \quad (9)$$

These coefficients cannot be interpreted as firing rates of real neurons; the  $A_\mu(t)$  have unlimited precision and can take on negative values. However, the relations between the  $A_\mu(t)$  will parallel the relations between the biologically-plausible firing rates  $a_i(t)$ . The amplitudes in the underlying space have biologically unrealistic properties which nonetheless are convenient for understanding the neural representation of a probabilistic model. In this section, we will develop methods to relate the mathematically convenient underlying space and the biologically plausible implementation of PDFs in the explicit space of model neurons.

## 2.2 Obtaining the Encoding Functions

Although we do not know the encoding functions at this point, we do know that they can be represented in terms of another set of basis functions  $\{\hat{\Phi}_\mu(x)\}$  through

$$\hat{\phi}_j(x) = \sum_{\mu} \hat{\kappa}_{j\mu} \hat{\Phi}_\mu(x) \quad (10)$$

where the coupling constants  $\hat{\kappa}_{j\mu}$  are in general distinct from the  $\kappa_{\nu i}$ . For many networks, it is appropriate to assume the basis for the encoders to be identical to the basis for the decoders. For example, in the case of the neural integrator (see section 2.5) the PDFs are continually mapped into and out of the underlying space provided by the

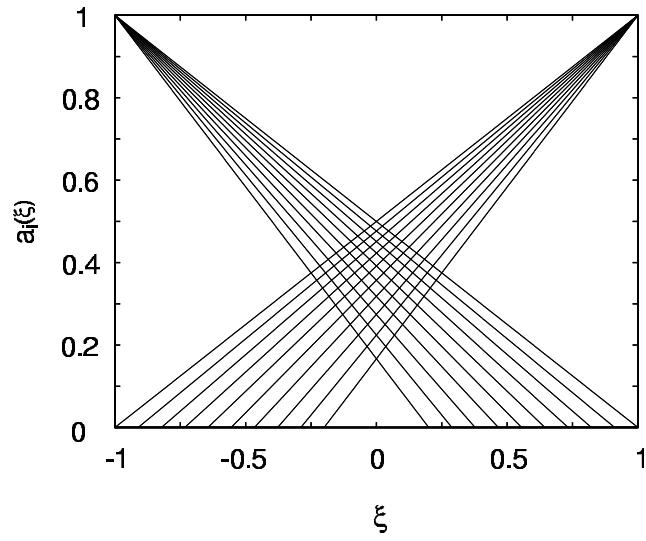


Figure 1: Broad piecewise-linear functions provide biologically-plausible neural firing rates. These firing profiles are similar to one-dimensional versions of the neural responses for Georgopoulos’s population vector.

$\Phi_\mu(x)$  and  $\hat{\Phi}_\nu(x)$ . Thus,  $\text{span}\{\Phi_\mu\}$  can be equal to  $\text{span}\{\hat{\Phi}_\nu\}$ . For definiteness, we take  $\Phi_\mu(x) = \hat{\Phi}_\mu(x)$ .

To find the encoding functions, we define the cost function

$$\begin{aligned} E_1 &= \frac{1}{2} \sum_i \int \left[ a_i(\mathbf{A}) - f \left( \int \hat{\phi}_i(x) \rho(x; \mathbf{A}) dx \right) \right]^2 \rho(\mathbf{A}) d\mathbf{A} \\ &= \frac{1}{2} \sum_i \int \left[ a_i(\mathbf{A}) - f \left( \sum_\nu \hat{\kappa}_{i\nu} \int \Phi_\nu(x) \rho(x; \mathbf{A}) dx \right) \right]^2 \rho(\mathbf{A}) d\mathbf{A} \end{aligned} \quad (11)$$

We now use gradient descent to determine the  $\hat{\kappa}_{i\nu}$  that minimize  $E_1$

$$\frac{d\hat{\kappa}_{j\mu}}{dt} \approx -\eta \frac{\partial E_1}{\partial \hat{\kappa}_{j\mu}} = \int (a_j(\mathbf{A}) - f(h_j(\mathbf{A}))) f'(h_j(\mathbf{A})) U_\mu(\mathbf{A}) \rho(\mathbf{A}) d\mathbf{A} \quad (12)$$

where we have defined

$$U_\nu(\mathbf{A}) = \int \Phi_\nu(x) \rho(x; \mathbf{A}) dx \quad (13)$$

$$h_j(\mathbf{A}) = \sum_\nu \hat{\kappa}_{j\nu} U_\nu(\mathbf{A}) \quad (14)$$

to simplify the expression.

To verify the efficacy of this learning rule, we apply it to a set of broadly-tuned, biologically-plausible neuronal responses to a precise input signal; in particular, we use piecewise-linear activities (Figure 1), similar to a one-dimensional version of Georgopoulos’s population vector, to define our neural responses over the interval  $[-1, 1]$  (see also Figure 4 in Fuchs *et al.*, 1988). We assume an underlying space spanned by two straight-line functions, shown in Figure 2a, and take the activation function to be rectification

$$f(x) = \begin{cases} x & x \geq 0 \\ 0 & x < 0 \end{cases} \quad (15)$$

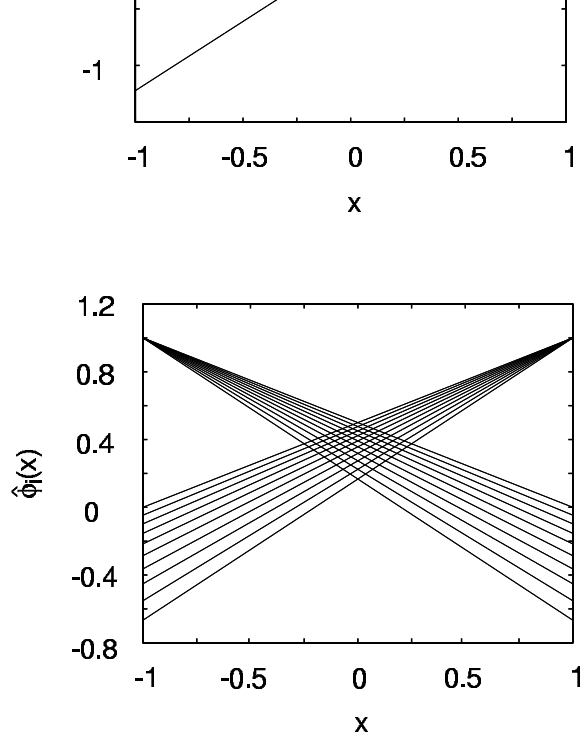


Figure 2: The learning rule yields effective encoders. (a) An orthonormal basis for the space underlying the piecewise-planar firing rates with linear encoders. Any line segment over the interval  $[-1, 1]$  can be expressed as a linear combination of these two basis functions. (b) Encoders found using the learning rule. For each neuron, the encoder has a slope identical to that of the firing rate profile.

Since we are interested in representing a precise input, we take  $\rho(x; t) = \delta(x - \xi(t))$ . Applying the learning rule, we obtain a set of encoders (Figure 2b) that are able to exactly reconstruct the neural activity patterns with input PDFs of the assumed Dirac delta function form.

As a second, more interesting test of this learning rule, we reconstruct the neural activity patterns with a very different basis set. We take the underlying space to be spanned by a collection of Gaussians (Figure 3a), but keep the same neural activity properties (Figure 1). After generating an orthonormal basis for the underlying space, we utilize the learning rule to find a set of encoding functions (Figure 3b).

The encoders obtained in this second approach have a complicated structure that would be difficult to deduce without an algorithm such as the learning rule derived above. However, these functions adequately reconstruct the neural activity patterns (Figure 3c), so our learning rule greatly expands the types of representations we can utilize.

Although the learning rule we have derived will minimize  $E_1$  in principle, it may yield a local minimum rather than the globally optimal solution. For example, since we typically use rectification for  $f$ , the derivative  $f'$  is a step function. An initially random set of parameters  $\hat{\kappa}_{j\mu}$  can produce  $h_j(\mathbf{A})$  that are always or almost always negative, so that the learning rule fails. A simple and effective correction is to add a small quantity (0.01 works reasonably well for the examples

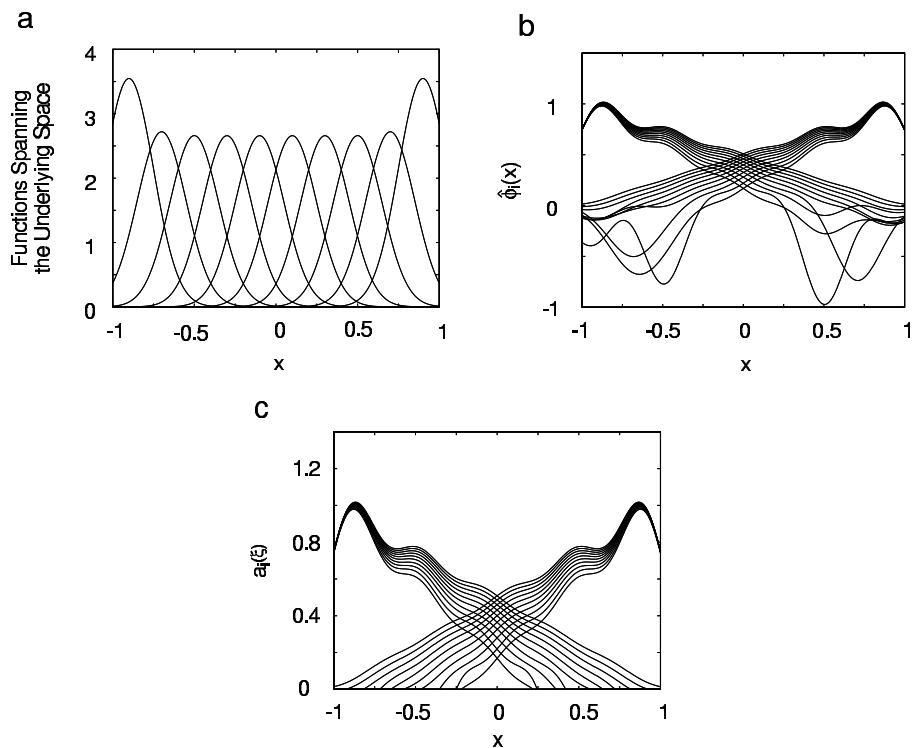


Figure 3: A second set of encoders found using the learning rule. (a) Gaussian functions spanning the underlying space. We convert these functions into an orthonormal basis for the underlying space before applying the learning rule. The underlying space is limited to the interval  $[-1, 1]$ , so the end-most Gaussians are truncated; the normalization constraint produces the increased maximum value observed here for these two functions. (b) Encoders found using the learning rule and the Gaussian-derived underlying space. These encoders relate broad firing rates to narrow PDF representations. (c) Firing rates determined from the encoders found with the learning rule and the Gaussian-derived underlying space. While the reconstruction is imperfect, the reconstructed firing rates correlate well with the assumed piecewise-linear firing rates.

considered) to  $f'(h_j(\mathbf{A}))$ .

### 2.3 Obtaining the Decoding Functions

We can make use of a similar procedure to find the decoding functions. Define

$$E_2 = \frac{1}{2} \iint \left( \rho(x; \mathbf{A}) - \sum_{i=1}^N a_i(\mathbf{A}) \phi_i(x) \right)^2 \rho(\mathbf{A}) dx d\mathbf{A} \quad (16)$$

Substituting equation 8 into this cost function

$$E_2 = \frac{1}{2} \iint \left( \rho(x; \mathbf{A}) - \sum_{i=1}^N a_i(\mathbf{A}) \sum_{\mu} \kappa_{\mu i} \Phi_{\nu}(x) \right)^2 \rho(\mathbf{A}) dx d\mathbf{A} \quad (17)$$

To find the  $\kappa_{\nu i}$  that minimize this cost function, we calculate

$$\frac{\partial E_2}{\partial \kappa_{\nu j}} = -M_{\nu j} + \sum_i \kappa_{\nu i} \Gamma_{ij} \quad (18)$$

where we define the matrices

$$M_{\nu j} = \iint \rho(x; \mathbf{A}) a_j(\mathbf{A}) \Phi_{\nu}(x) \rho(\mathbf{A}) dx d\mathbf{A} \quad (19)$$

and

$$\Gamma_{ij} = \int a_i(\mathbf{A}) a_j(\mathbf{A}) \rho(\mathbf{A}) d\mathbf{A} \quad (20)$$

From here, we can find the  $\kappa_{\nu i}$  by using gradient decent to generate a learning rule. Alternatively, we can set  $\partial E_2 / \partial \kappa_{\nu j} = 0$  and solve for  $\kappa_{\nu j}$ , yielding

$$\kappa = \Gamma^{-} M \quad (21)$$

where  $\Gamma^{-}$  denotes the pseudo-inverse of  $\Gamma$ .

Making use of this procedure to determine decoders for neurons with piecewise-linear activity patterns using the basis shown in Figure 2a (discussed in section 2.2) reveals a shortcoming of the algorithm. This algorithm produces two decoders that play a significant role (Figure 4a), with the other decoders nearly zero (Figure 4b). These decoders require neurons that are extremely precise in their firing rates, rather than making use of redundant neurons to improve the quality of the representation. To overcome this problem, we must account for the limited precision of neural firing rates by considering noise.

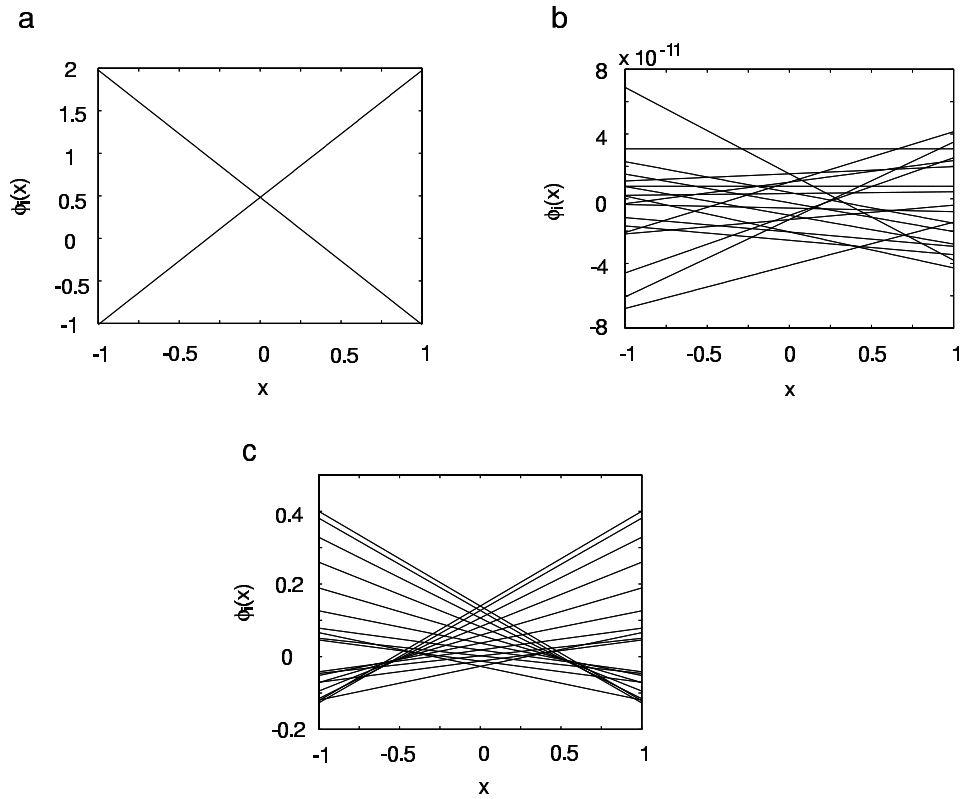


Figure 4: Decoders obtained from the linear underlying space basis functions (figure 2a). (a) and (b) These decoders require neurons of extreme precision to operate properly. Two decoders (a) significantly contribute to the decoded PDFs, while the other decoders (b) are nearly zero, contributing little or nothing to the decoded PDF. (c) Decoders obtained from the linear underlying space basis functions (figure 2a), assuming a small amount of noise in the neurons. The decoders shown here result from a noise variance of 0.01, limiting the precision of the neurons to biologically-plausible levels. Note that these decoders can take on negative values, so the decoded functions may only approximate the encoded PDF.

## 2.4 Coping With Noise

The procedures described above can be extended to account for the limited precision of neural firing rates and for any intrinsic noise of real neurons. We convert the neural firing rates into stochastic processes

$$a_i(\mathbf{A}) \rightarrow a_i(\mathbf{A}) + \eta_i \quad (22)$$

where  $\eta_i$  is the noise source.

To ensure that the encoders and decoders found are not dependent on a particular realization of the noise, we alter the cost functions

$$E_1 = \frac{1}{2} \left\langle \sum_i \int \left( (a_i(\mathbf{A}) + \eta_i) - f \left( \int \hat{\phi}_i(x) \rho(x; \mathbf{A}) dx \right) \right)^2 \rho(\mathbf{A}) d\mathbf{A} \right\rangle_{\{\eta_i\}} \quad (23)$$

$$E_2 = \frac{1}{2} \left\langle \iint \left( \rho(x; \mathbf{A}) - \sum_{i=1}^N (a_i(\mathbf{A}) + \eta_i) \phi_i(x) \right)^2 \rho(\mathbf{A}) dx d\mathbf{A} \right\rangle_{\{\eta_i\}} \quad (24)$$

Here, the angle brackets indicate an ensemble average over the neuronal noises  $\{\eta_i\}$ .

Repeating the above calculations, we find the derivatives  $\partial E_1 / \partial \kappa_{\mu j}$  and  $\partial E_2 / \partial \hat{\kappa}_{i\nu}$ . Taking the  $\eta_i$  to be independent, identically distributed, zero-mean Gaussian noise with variance  $\sigma^2$  leaves  $\partial E_1 / \partial \hat{\kappa}_{i\nu}$  (and, thus, the encoders) unchanged, but

$$\begin{aligned} \frac{\partial E_2}{\partial \kappa_{\nu j}} &= - \iint \rho(x; \mathbf{A}) a_j(\mathbf{A}) \Phi_\nu(x) dx \rho(\mathbf{A}) d\mathbf{A} \\ &\quad + \sum_i \kappa_{\nu i} \left[ \int a_i(\mathbf{A}) a_j(\mathbf{A}) \rho(\mathbf{A}) d\mathbf{A} + \sigma^2 \delta_{ij} \right] \end{aligned} \quad (25)$$

Setting these derivatives to zero and re-expressing as a matrix equation, we have

$$(\Gamma + \sigma^2 I) \kappa = M \quad (26)$$

where  $\Gamma$  and  $M$  are as defined in equations 19 and 20. We can solve directly for  $\kappa$  by inverting  $(\Gamma + \sigma^2 I)$ .

In section 2.3, we generated decoders that constrain the dimensionality of the underlying space. The example we considered, however, effectively utilizes only two of the neurons and required those neurons to have unrealistically precise firing rates. Using the method developed above, we determine a set of decoders that utilizes all of the neurons in the representation (Figure 4c) and eliminates the need for unrealistically precise firing rates.

## 2.5 A Neural Integrator Model

An example of a neural integrator is the group of neurons that hold the eyes in a fixed position in the absence of visual input. These recurrently-connected neurons are able to hold the eye in position for times much longer than the interspike interval of the neurons; collectively, they are an attractor network that acts as a memory of eye position which lasts for several seconds (Seung, 1996).

By introducing temporal dynamics into the underlying probabilistic models, we can create a model of a neural integrator. The dynamics are straightforward: for a short time  $\tau$ , the PDF should be unchanged, so

$$\rho(x; t + \tau) = \rho(x; t) \quad (27)$$

where  $x$  is the value (i.e. eye position) stored in the memory.

As discussed above, we generate decoding functions using piecewise-linear activities, linear encoders, and a rectifying activation function. Making use of this representation, the encoding and decoding rules (equations 5 and 6), and the probabilistic dynamics (equation 27), we can show

$$a_i(t + \tau) = g \left( \int \hat{\phi}_i(x) \rho(x; t + \tau) dx \right) \quad (28)$$

$$= g \left( \sum_j a_j(t) \int \hat{\phi}_i(x) \phi_j(x) dx \right) \quad (29)$$

Defining

$$\omega_{ij} = \int \hat{\phi}_i(x) \phi_j(x) dx \quad (30)$$

we may rewrite this as

$$a_i(t + \tau) = g \left( \sum_j \omega_{ij} a_j(t) \right) \quad (31)$$

The recurrent neural network that results is fully connected, with each neuron having a synaptic connection to every other neuron.

The stored value of the eye position is extracted by calculating the expectation value of the random variable  $x$ , weighted by the decoded PDF. Ideally, we would like any value in the supported range to be held constant, so that the network functions as a line attractor (Seung, 1996), a kind of continuous attractor. However, the system actually operates as a collection of point attractors with only a limited number of stable fixed points, as can be seen from the network's transfer function (Figure 5). The structure of the transfer function, and the number of stable fixed points, depends on the dimensionality

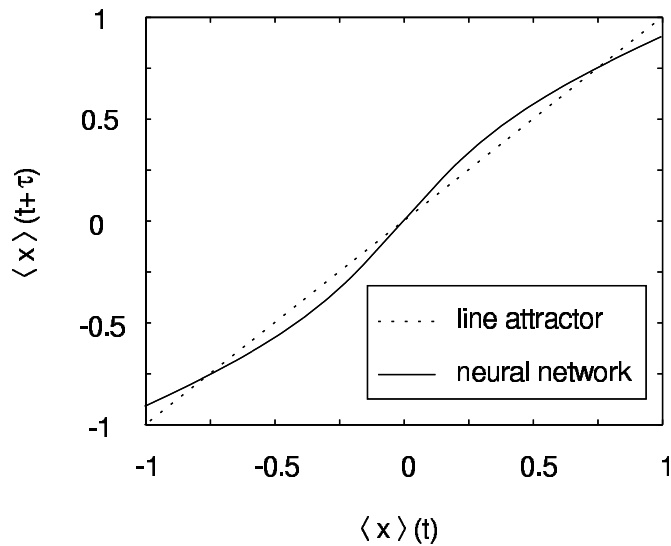


Figure 5: The neural integrator model maintains only a limited number of values, rather than any input value. The number of stable fixed points of the neural integrator model can be seen in the network’s transfer function. Here there are two stable fixed points for a neural integrator consisting of 20 neurons with decoders found using two basis functions in the underlying space.

$D$  of the underlying space. As the dimensionality of the underlying space is increased, the neural integrator can support additional stable fixed points, eventually approximating a line attractor. This neural integrator model is essentially a variation of the model constructed by Eliasmith and Anderson (1999).

### 3 Probabilistic Inference Performed by Neural Networks

#### 3.1 Inference

Inference between two related variables in the implicit space, say from an input  $x$  to an output  $y$ , is performed by taking a weighted average of the conditional probability  $\rho(y|x)$

$$\rho(y;t) = \int \rho(y|x)\rho(x;t)dx \tag{32}$$

We have assumed in equation 32 that the relationship between  $x$  and  $y$  is independent of the values of the underlying parameters, so

$$\rho(y|x; \{A_\mu(t)\}) = \rho(y|x) \tag{33}$$

This assumption fixes the structure of the probabilistic model, explicitly excluding learning from any neural networks derived from it. The conditional probability  $\rho(y|x)$  is like a fixed look-up-table; the Marr-Albus theory of cerebellar function can be directly mapped into equation 32 (Hakimian *et al.*, 1999).

Using this relation and representations of the form discussed above, we have

$$\rho(x; t) = \sum_i a_i(t) \phi_i(x) \quad (34)$$

$$a_i(t) = f \left( \int \hat{\phi}_i(x) \rho(x; t) dx \right) \quad (35)$$

$$\rho(y; t) = \sum_j b_j(t) \psi_j(y) \quad (36)$$

$$b_j(t) = g \left( \int \hat{\psi}_j(y) \rho(y; t) dy \right) \quad (37)$$

leading to

$$b_j(t) = g \left( \sum_i w_{ji} a_i(t) \right) \quad (38)$$

with the coupling coefficients

$$w_{ji} = \iint \hat{\psi}_j(y) \rho(y|x) \phi_i(x) dx dy \quad (39)$$

With well-chosen encoding and decoding functions, equations 38 and 39 allow us to construct a neural network with the desired relationship between the implicit variables, rather than using a training procedure to find a relation from a data set.

This approach to inference is naturally extended to greater numbers of implicit variables. For example, suppose we add a second input  $z$  to the above network. We then write

$$\rho(y; t) = \iiint \rho(y|x, z) \rho(x; t) \rho(z; t) dx dz \quad (40)$$

Representing  $z$  using

$$\rho(z; t) = \sum_k c_k(t) \theta_k(z) \quad (41)$$

$$c_k(t) = f \left( \int \hat{\theta}_k(z) \rho(z; t) dz \right) \quad (42)$$

leads to

$$b_j(t) = g \left( \sum_i w_{jik} a_i(t) c_k(t) \right) \quad (43)$$

with

$$w_{jik} = \iiint \hat{\psi}_j(y) \rho(y|x, z) \phi_i(x) \theta_k(z) dx dy dz \quad (44)$$

An interesting feature of this neural network is that it functions by using multiplicative interactions. This multiplication is assumed to

take place by coincidence detection in the dendrites; the implication is that the dendrites are active processing elements (Mel, 1994; Cash and Yuste, 1998).

The structure of the neural network in the explicit space depends strongly upon the structure assumed for the underlying probabilistic model in the implicit space. This probabilistic basis leads to useful connections to Bayesian belief networks (section 4).

### 3.2 A Communication Channel Model

As a concrete example, we now use equations 38 and 39 to implement a communication channel. Specifically, we wish to encode a single input value  $\xi(t)$  as a PDF  $\rho(x;t)$  represented by a population of neurons, and copy that PDF into another PDF  $\rho(y;t)$  represented by a second population of neurons. To extract a unique output value from  $\rho(y;t)$ , we focus on the expectation value of  $y$ . We use 20 neurons to represent the input PDF  $\rho(x;t)$  and 16 neurons to represent the output PDF  $\rho(y;t)$ . The encoders and decoders for these neurons are generated from two straight-line basis functions (Figure 2a) and piecewise-linear neural responses as discussed previously (sections 2.2 and 2.4).

Since we only want to encode a single value, and not a complex multimodal distribution, we assume the input PDF is of the form  $\rho(x;t) = \delta(x - \xi(t))$ . Our goal is to accurately reproduce this input, so we take the conditional PDF to be  $\rho(y|x) = \delta(y - x)$ .

To interpret the performance of the neural network, we compare the expectation value  $\langle y \rangle$  of the random variable  $Y$ , weighted by the PDF decoded from the network outputs  $\{b_j(t)\}$ , to the input  $\xi$ . The decoded PDF is a weighted sum of linear decoding functions, and is thus a straight line itself. This is of course a poor reproduction of the Dirac delta function input, but  $\langle y \rangle$  is closely in accord with the input values (fig 6).

### 3.3 Working in the Underlying Space

So far, we have used the concept of the underlying space as a tool for developing the encoders and decoders. However, we also can make direct use of the underlying space to set up abstract networks, then convert those into networks of real neurons. To accomplish this, we derive relations between the firing rates in the two spaces ( $\{A_\mu(t)\}$  and  $\{a_i(t)\}$ ). The neural network in the explicit space then constitutes a physical implementation of the abstract network in the underlying space. The issues of the role of neuronal firing rate variability in the population code (see for example Abbott and Dayan, 1999) may thus be separated from the issues of the propagation of probabilistic information.

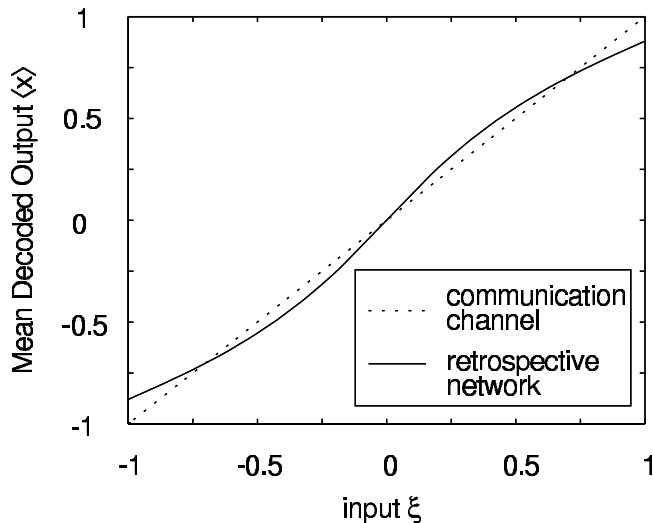


Figure 6: Although the PDF is not accurately represented, the mean value of the PDF can be satisfactorily retrieved from the neural network. By using only two basis functions to generate the decoders, the output PDFs are elements of a space of dimension two. This is suitable for representing the total weight and the mean of the PDF, but not higher moments of the PDFs.

First, consider the decoding rule

$$\rho(x; t) = \sum_{\mu} A_{\mu}(t) \Phi_{\mu}(x) = \sum_i a_i(t) \phi_i(x) \quad (45)$$

Making use of equation 8,

$$\sum_{\mu} A_{\mu}(t) \Phi_{\mu}(x) = \sum_i a_i(t) \sum_{\nu} \kappa_{\nu i} \Phi_{\nu}(x) \quad (46)$$

Since the  $\Phi_{\mu}(x)$  are orthonormal functions, we have

$$A_{\mu}(t) = \sum_i \kappa_{\nu i} a_i(t) \quad (47)$$

or

$$A = \kappa a \quad (48)$$

when written as a matrix equation.

Next, consider the encoding rule

$$a_i(t) = f \left( \int \hat{\phi}_i(x) \rho(x; t) dx \right) \quad (49)$$

Recalling that  $\hat{\phi}_i(x) = \sum_{\nu} \hat{\kappa}_{i\nu} \Phi_{\nu}(x)$  and  $A_{\nu}(t) = \int \Phi_{\nu}(x) \rho(x; t) dx$ , we have

$$\begin{aligned} a_i(t) &= f \left( \int \sum_{\nu} \hat{\kappa}_{i\nu} \Phi_{\nu}(x) \rho(x; t) dx \right) \\ &= f \left( \sum_{\nu} \hat{\kappa}_{i\nu} A_{\nu}(t) \right) \end{aligned} \quad (50)$$

Writing this in matrix form,

$$a = f(\hat{\kappa}A) \quad (51)$$

where the generalization of the activation function  $f()$  acts on the individual elements of its vector argument.

As a demonstration of the use of the underlying space to set up neural networks, we return again to the  $X \rightarrow Y$  inference network and implement a communication channel with 20 input neurons and 16 output neurons. We take the underlying spaces for both the input  $x$  and the output  $y$  to be defined by linear functions over the interval  $[-1, 1]$ , with bases of the form shown in Figure 2a. The associated PDFs are represented using

$$\rho(x; t) = \sum_{\mu} A_{\mu}(t) \Phi_{\mu}(x) \quad (52)$$

$$\rho(y; t) = \sum_{\nu} B_{\nu}(t) \Psi_{\nu}(y) \quad (53)$$

With these representations, the probabilistic relation

$$\rho(y; t) = \int \rho(y|x) \rho(x; t) dx \quad (54)$$

becomes

$$B_{\nu}(t) = \sum_{\mu} \Omega_{\nu\mu} A_{\mu}(t) \quad (55)$$

where

$$\Omega_{\nu\mu} = \int \Psi_{\nu}(y) \rho(y|x) \Phi_{\mu}(x) dx dy \quad (56)$$

We next convert this into a neural network in the explicit space, according to

$$b_j(t) = g \left( \sum_{\nu} \hat{\kappa}_{j\nu}^{(y)} B_{\nu}(t) \right) \quad (57)$$

$$= g \left( \sum_{\nu} \hat{\kappa}_{j\nu}^{(y)} \sum_{\mu} \Omega_{\nu\mu} A_{\mu}(t) \right) \quad (58)$$

$$= g \left( \sum_{\nu} \hat{\kappa}_{j\nu}^{(y)} \sum_{\mu} \Omega_{\nu\mu} \sum_i \kappa_{\mu i}^{(x)} a_i(t) \right) \quad (59)$$

$$= g \left( \sum_i \sum_{\mu, \nu} \hat{\kappa}_{j\nu}^{(y)} \Omega_{\nu\mu} \kappa_{\mu i}^{(x)} a_i(t) \right) \quad (60)$$

By identifying

$$\omega_{ji} = \sum_{\mu, \nu} \hat{\kappa}_{j\nu}^{(y)} \Omega_{\nu\mu} \kappa_{\mu i}^{(x)} \quad (61)$$

we may rewrite equation 60 as

$$b_j(t) = g \left( \sum_i \omega_{ji} a_i(t) \right) \quad (62)$$

This alternate derivation yields a neural network with the same feed-forward rule (equation 38) and the same synaptic weights found previously (equation 39).

Although this example only reproduces results previously found, there are significant advantages to working in the underlying space. Perhaps most importantly, the fundamental structure of neural networks is made more transparent by eliminating the redundancies that arise in the networks due to the limited representational ability of neurons. Significantly, we see that computational properties of the nonlinear update rule for the output neurons (equation 60) can be understood by studying the linear update rule in the underlying space (equation 55).

## 4 Neural Belief Networks

### 4.1 Bayesian Belief Networks

So far, we have developed methods for encoding and decoding probability density functions into and from the firing rates of populations of neurons. This was done by focusing on encoding either a single random variable, or examining the behavior of a few variables interacting in a straightforward way. However, we do not wish to restrict ourselves to only the simplest implicit spaces.

In this section, we will explore ways in which we can apply the methods so far developed to more complicated implicit spaces. In particular, we will use Bayesian belief networks to efficiently organize the implicit random variables, and then use these Bayesian belief networks to generate neural networks.

Bayesian belief networks are directed acyclic graphs that represent probabilistic models (Figure 7). Each node represents a random variable, and the arcs signify the presence of direct causal influences between the linked variables. The strengths of these influences are defined using conditional probabilities. The directionality of a specified link indicates the direction of causality (or, more simply, relevance); an arc points from direct cause to effect.

Bayesian belief networks have two properties that we will find very useful, both of which stem from the independencies shown by the graph structure. First, the value of a node  $X$  is not dependent upon all of the other graph nodes. Rather, it depends only on a subset of the nodes, called a Markov blanket of  $X$ , that separates node  $X$  from all

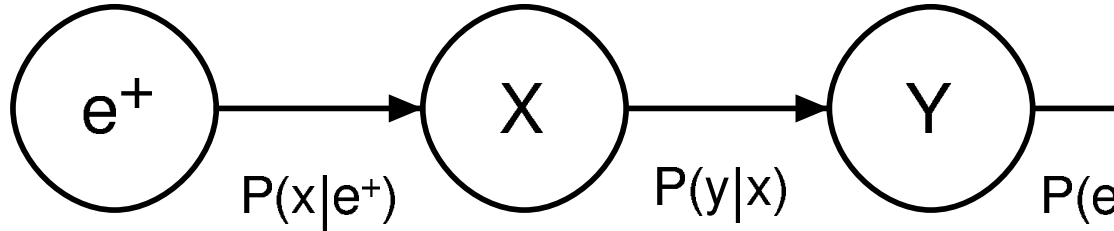


Figure 7: A chain-structured Bayesian belief network. Evidence  $e^+$  and  $e^-$  from the two ends of the chain influences the belief in the random variables  $X$  and  $Y$ . In a straightforward terminology,  $X$  is referred to as the parent of  $Y$  and  $Y$  the child of  $X$ . From the structure of the graph, we can see for example that  $Y$  is conditionally independent of  $e^+$  given  $X$ ; this is true regardless of the values of the links  $P(e^-|y)$ ,  $P(y|x)$ , and  $P(x|e^+)$ .

the other nodes in the graph. The Markov blanket of interest to us can be readily determined from the graph structure. It is comprised of the union of the direct parents of  $X$ , the direct successors of  $X$ , and all direct parents of the direct successors of  $X$ . Second, the joint probability over the random variables is decomposable

$$P(x_1, x_2, \dots, x_n) = \prod_{i=1}^n P(x_i | \text{Pa}(x_i)) \quad (63)$$

where  $\text{Pa}(x_i)$  denotes the (possibly empty) set of direct parent nodes of  $X_i$ . This decomposition comes about from repeated application of Bayes' rule and from the structure of the graph. We will make extensive use of both these properties.

## 4.2 Encoding Bayesian Belief Networks Into Neural Networks

The neural networks we have introduced above as examples may be viewed as simple Bayesian belief networks. For example, the implicit space for the communication channel is represented by a directed acyclic graph consisting of two connected nodes (Figure 8a). This same graph also represents any probabilistic model where a single random variable is inferred from one source of evidence.

It is enlightening to reconsider this inference problem in terms of a Bayesian belief network. For convenience, we will work in the underlying space. Our objective is to find the most likely marginal PDFs  $\rho(y; t)$  and  $\rho(x; t)$  to describe the system. We represent these PDFs as

$$\rho(x; t) = \sum_{\mu} A_{\mu}(t) \Phi_{\mu}(x) \quad (64)$$

$$\rho(y; t) = \sum_{\nu} B_{\nu}(t) \Psi_{\nu}(y) \quad (65)$$

The joint probability for the PDFs thus depends on the parameters  $\{A_\mu(t)\}$  and  $\{B_\nu(t)\}$ , so we must maximize  $P(\rho(x;t), \rho(y;t))$  with respect to these parameters (the firing rates of the metaneurons). In this network, we need to find values of the output firing rates  $\{B_\nu(t)\}$  only, since the input firing rates are assumed to be fully determined by an encoding process.

We can rewrite the joint probability as

$$P(\rho(x;t), \rho(y;t)) = P(\rho(y;t) | \rho(x;t)) P(\rho(x;t)) \quad (66)$$

To reproduce the previous results, we define a cost function by

$$\begin{aligned} E_y &= \frac{1}{2} \int \left( \rho(y;t) - \int \rho(y|x) \rho(x;t) dx \right)^2 dy \\ &= \frac{1}{2} \int \left( \sum_\nu B_\nu(t) \Psi_\nu(y) - \sum_\mu A_\mu(t) \int \rho(y|x) \Phi_\mu(x) dx \right)^2 dy \end{aligned} \quad (67)$$

and assume the conditional probability  $P(\rho(y;t) | \rho(x;t))$  has the form of a Gibbs distribution, i.e.

$$P(\rho(y;t) | \rho(x;t)) = N_y e^{-\beta_y E_y} \quad (68)$$

The inverse ‘‘temperature’’  $\beta_y$  is irrelevant in this case, but could have significance in more general Bayesian belief networks. Further,  $P(\rho(x;t))$  will prove to be unimportant.

To maximize  $P(\rho(x;t), \rho(y;t))$ , we first note that wherever the joint probability  $P(\rho(x;t), \rho(y;t))$  has a maximum, the associated log-likelihood  $L = \log P(\rho(x;t), \rho(y;t))$  also has a maximum. Because of the product of distributions in equation 66 and the Gibbs form of the conditional probability factor, it is convenient to use the log-likelihood in finding the parameters that maximize the joint probability. We calculate the derivatives

$$\begin{aligned} \frac{\partial L}{\partial B_\nu} &= \frac{\partial}{\partial B_\nu} \log (P(\rho(x;t) | \rho(y;t)) P(\rho(x;t))) \\ &= \frac{\partial}{\partial B_\nu} \log P(\rho(x;t) | \rho(y;t)) \\ &= -\beta_y \frac{\partial E_y}{\partial B_\nu} \end{aligned} \quad (69)$$

Using gradient ascent to find the maximum, we obtain the update rule

$$\begin{aligned} \frac{dB_\nu(t)}{dt} &= -\eta \beta_y \frac{\partial E_y}{\partial B_\nu} \\ &= -\eta \beta_y \left( B_\nu(t) - \sum_\mu \Omega_{\nu\mu} A_\mu(t) \right) \end{aligned} \quad (70)$$

where

$$\Omega_{\nu\mu} = \iint \Psi_\nu(y)\rho(y|x)\Phi_\mu(x)dx dy \quad (71)$$

In applying gradient ascent, we have introduced another parameter  $\eta$ ; the value of the temperature parameter  $\beta_y$  thus becomes unimportant here.

Equation 70 has a fixed point at

$$B_\nu(t) = \sum_\mu A_\mu(t) \iint \Psi_\nu(y)\rho(y|x)\Phi_\mu(x)dx dy \quad (72)$$

This is identical to previously obtained relations for inference, notably equation 55).

We can use a similar strategy to develop neural network update rules for arbitrary Bayesian belief networks. Assume the Bayesian belief network consists of  $N$  nodes, representing random variables  $X_1, X_2, X_3, \dots, X_N$ . Taking the graph structure to also represent the causal relations between the marginal distributions, we can write the joint probability of the marginals, which we will denote  $\mathcal{P}$ , as

$$\begin{aligned} \mathcal{P} &= P\left(\rho(x_1;t), \rho(x_2;t), \dots, \rho(x_N;t)\right) \\ &= \prod_{i=1}^N P\left(\rho(x_i;t) \mid \{\rho(x_j;t) : X_j \in \text{Pa}(X_i)\}\right) \end{aligned} \quad (73)$$

where  $\text{Pa}(X_i)$  denotes the set of all direct parents of the node representing  $X_i$  in the Bayesian belief network. Nodes that have no parents, referred to here as root nodes, will be present as well; these nodes constitute priors on the PDFs. We will generally take these to be uniform over the class of PDFs that can be represented, having no effect on the dynamics to be developed below.

We introduce representations

$$\rho(x_i;t) = \sum_\mu A_\mu^{(i)}(t)\Phi_\mu^{(i)}(x_i) \quad (74)$$

for the marginal distributions in the underlying space. Making use of these representations, we define the cost functions

$$\begin{aligned} E_i &= \frac{1}{2} \int \left( \rho(x_i;t) - \int \rho(x_i|\text{Pa}(x_i)) \prod_j \rho(x_j;t) dx_j \right)^2 dx_i \\ &= \frac{1}{2} \int \left( \sum_\mu A_\mu^{(i)}(t)\Phi_\mu^{(i)}(x_i) - \int \rho(x_i|\text{Pa}(x_i)) \prod_j \sum_{\nu_j} A_{\nu_j}^{(j)}(t)\Phi_{\nu_j}^{(j)}(x_j) dx_j \right)^2 dx_i \end{aligned}$$

(75)

where the index  $j$  for the product runs over the direct parents of  $X_i$ . We take the conditional probabilities for the PDFs to be Gibbs distributions

$$P(\rho(x_i; t) | \{\rho(x_j; t) : X_j \in \text{Pa}(X_i)\}) = N_i e^{-\beta_i E_i} \quad (76)$$

with these cost functions.

To maximize the joint probability  $\mathcal{P}$ , we again focus on the log-likelihood

$$\log \mathcal{P} = \sum_{i=1}^N \log P(\rho(x_i; t) | \{\rho(x_j; t) : X_j \in \text{Pa}(X_i)\}) \quad (77)$$

which, for the Gibbs distributions we are assuming, becomes

$$\log \mathcal{P} = \sum_{i=1}^N \log N_i - \sum_{i=1}^N \beta_i E_i \quad (78)$$

Employing gradient ascent to maximize  $\log \mathcal{P}$ ,

$$\begin{aligned} \frac{dA_\sigma^{(k)}}{dt} &= \eta \frac{\partial}{\partial A_\sigma^{(k)}} \log \mathcal{P} \\ &= -\eta \sum_{i=1}^N \beta_i \frac{\partial E_i}{\partial A_\sigma^{(k)}} \end{aligned} \quad (79)$$

Since  $A_\sigma^{(k)}$  does not appear in all of the cost functions,  $\partial E_i / \partial A_\sigma^{(k)}$  is nonzero only for  $i = k$  and when the graph node for  $X_i$  is one of the direct children of the graph node for  $X_k$ . Thus,

$$\frac{1}{\eta} \frac{dA_\sigma^{(k)}}{dt} = -\beta_k \frac{\partial E_k}{\partial A_\sigma^{(k)}} - \sum_{i \in \{i: X_i \in \text{Ch}(X_k)\}} \beta_i \frac{\partial E_i}{\partial A_\sigma^{(k)}} \quad (80)$$

As was the case for the two-node inference network, the input PDF or PDFs will be specified by an encoding process rather than an update rule of this sort.

The derivatives in equation 80 are straightforward but lengthy to evaluate. We omit the details of the calculation and simply state the

results

$$\begin{aligned}
\frac{1}{\eta} \frac{dA_\sigma^{(k)}}{dt} = & \\
& -\beta_k \left( A_\sigma^{(k)} - \prod_j \sum_{\nu_j} A_{\nu_j}^{(j)} \Omega_{\sigma\nu_1\nu_2\cdots\nu_{jmax}}^{(k)} \right) \\
& + \sum_i \beta_i \sum_\mu A_\mu^{(i)} \prod_{j \neq k} \sum_{\nu_j} A_{\nu_j}^{(j)} \Omega_{\mu\nu_1\nu_2\cdots\nu_{jmax}}^{(ik)} \sigma \\
& - \sum_i \beta_i \prod_j \prod_{j' \neq k} \sum_{\nu_j} A_{\nu_j}^{(j)} \sum_{\mu_{j'}} A_{\mu_{j'}}^{(j')} \Upsilon_{\nu_1\nu_2\cdots\nu_{jmax} \mu_1\mu_2\cdots\mu_{j'max}}^{(jj'k)} \sigma \quad (81)
\end{aligned}$$

where we have defined

$$\begin{aligned}
\Omega_{\sigma\nu_1\nu_2\cdots\nu_{jmax}}^{(k)} = & \\
& \int \Phi_\sigma^{(k)}(x_k) \rho(x_k | \text{Pa}(x_k)) \prod_j \Phi_{\nu_j}^{(j)}(x_j) dx_j dx_k \quad (82)
\end{aligned}$$

$$\begin{aligned}
\Omega_{\mu\nu_1\nu_2\cdots\nu_{jmax}}^{(ik)} \sigma = & \\
& \int \Phi_\mu^{(i)}(x_i) \rho(x_i | \text{Pa}(x_i)) \Phi_\sigma^{(k)}(x_k) \prod_{j \neq k} \Phi_{\nu_j}^{(j)}(x_j) dx_j dx_i dx_k \quad (83)
\end{aligned}$$

and

$$\begin{aligned}
\Upsilon_{\nu_1\nu_2\cdots\nu_{jmax} \mu_1\mu_2\cdots\mu_{j'max}}^{(jj'k)} \sigma = & \\
& \int \left( \int \Phi_\sigma^{(k)}(x_k) \rho(x_i | \text{Pa}(x_i)) \prod_{j' \neq k} \Phi_{\mu_{j'}}^{(j')}(x_{j'}) dx_{j'} dx_k \right. \\
& \left. \int \rho(x_i | \text{Pa}(x_i)) \prod_j \Phi_{\nu_j}^{(j)}(x_j) dx_j \right) dx_i \quad (84)
\end{aligned}$$

The sums over the index  $i$  in equation 81 run over the children of  $X_k$ . The products are over the parents of either node  $X_k$  (equation 82, first term in 81) or node  $X_i$  (equations 83 and 84, second and third term in 81), possibly excluding node  $X_k$  itself. From these equations, it can be seen that the PDF represented at a node  $X_i$  is updated based only on its direct parents, its direct descendents, and the direct parents of its direct descendents, so that  $X_i$  is separated from all other nodes in the neural belief networks by an appropriate Markov blanket.

Equations 81 through 84 can be awkward to use directly. It can be more convenient to write out the cost functions for a specific probabilistic model using equation 75 and directly evaluate the necessary derivatives (specified by equation 80).

### 4.3 Inference in Neural Belief Networks

The method developed above for generating neural networks produces networks with some new dynamical properties. For example, the  $X \rightarrow Y$  inference network (equation 70) has fixed points (equation 72) that reproduce the previous relations for this type of network. However, we will see that the network also has properties similar to those of attractor networks, such as the neural integrator we examined previously (section 2.5).

Attractor networks are able to maintain steady values over long periods of time. Neural networks based on probabilistic inference are able to adjust activity levels rapidly to reflect a changing input. Surprisingly, these two types of networks can be combined in a straightforward manner in a large number of cases, allowing for gradual changes in a represented PDF.

An attractor network is an implementation of the simple relationship

$$\rho(y; t + \tau) = \rho(y; t) \quad (85)$$

for small  $\tau$ , with most of the complexity coming from the neural representation of the PDF. We can allow for gradual changes in  $\rho(y; t)$  due to an input  $X$  by means of

$$\rho(y; t + \tau) = \rho(y; t) + \epsilon (\rho_{\text{ext}}(y; t) - \rho(y; t)) \quad (86)$$

The external signal  $\rho_{\text{ext}}(y; t)$  is

$$\rho_{\text{ext}}(y; t) = \int \rho(y|x)\rho(x; t)dx \quad (87)$$

The value of the parameter  $\epsilon$  determines the rate at which changes in  $\rho(x; t)$  become incorporated into  $\rho(y; t)$ . The value of  $\epsilon$  can range between 0, corresponding to an attractor network, and 1, corresponding to probabilistic inference only.

Substitution of the representations

$$\rho(x; t) = \sum_{\mu} A_{\mu}(t)\Phi_{\mu}(x) \quad (88)$$

$$\rho(y; t) = \sum_{\nu} B_{\nu}(t)\Psi_{\nu}(y) \quad (89)$$

leads to

$$B_{\nu}(t+\tau) = B_{\nu}(t) + \epsilon \left( \sum_{\mu} A_{\mu}(t) \iint \Psi_{\nu}(y)\rho(y|x)\Phi_{\mu}(x)dxdy - B_{\nu}(t) \right) \quad (90)$$

Since  $\tau$  is small, we expand

$$B_\nu(t + \tau) = B_\nu(t) + \tau \frac{dB_\nu(t)}{dt} + O(\tau^2) \quad (91)$$

Keeping terms to first order and simplifying, we find

$$\frac{dB_\nu(t)}{dt} = -\frac{\epsilon}{\tau} \left( B_\nu(t) - \sum_\mu A_\mu(t) \iint \Psi_\nu(y) \rho(y|x) \Phi_\mu(x) dx dy \right) \quad (92)$$

Comparing equations 70 and 92, we see that they are identical when we define the parameters such that  $\epsilon/\tau = \eta\beta_y = K_y$ .

We can readily convert the update rule in the underlying space into a neural network in the explicit space. Recalling equation 51, we have

$$b_i(t + \tau) = g \left( \sum_\nu \hat{\kappa}_{i\nu}^{(y)} B_\nu(t + \tau) \right) \quad (93)$$

where  $b_i(t)$  are the firing rates in the explicit space for  $Y$  and  $g$  and the coefficients  $\hat{\kappa}_{i\nu}^{(y)}$  define the mapping from the underlying space to the explicit space. Substituting equation 90 into equation 93, we obtain

$$b_j(t + \tau) = g \left( \sum_i \lambda_{ji} b_i(t) + \sum_i \omega_{ji} a_i(t) \right) \quad (94)$$

with

$$\lambda_{ji} = (1 - \epsilon) \sum_\mu \hat{\kappa}_{j\mu}^{(y)} \kappa_{\mu i}^{(y)} \quad (95)$$

$$\omega_{ji} = \epsilon \sum_{\mu, \nu} \hat{\kappa}_{j\mu}^{(y)} \left( \iint \Psi_\mu(y) \rho(y|x) \Phi_\nu(x) dx dy \right) \kappa_{\nu i}^{(x)} \quad (96)$$

The neural network thus constructed combines properties of the two types of networks (inference and attractor) previously discussed. It has feedforward connections  $\omega_{ji}$  from an input  $X$  driving an output  $Y$ , but  $Y$  has recurrent connections  $\lambda_{ji}$  that try to preserve a steady value (Figure 8b).

#### 4.4 Predictive and Retrospective Support

Neural belief networks can feature two distinct types of information propagation that provide support for the PDFs represented at each graph node. Predictive support, also called causal support, is probabilistic information that propagates, along the directions of the graph links, from cause to effect (Pearl, 1988). The network considered in section 4.3 involves only predictive support.

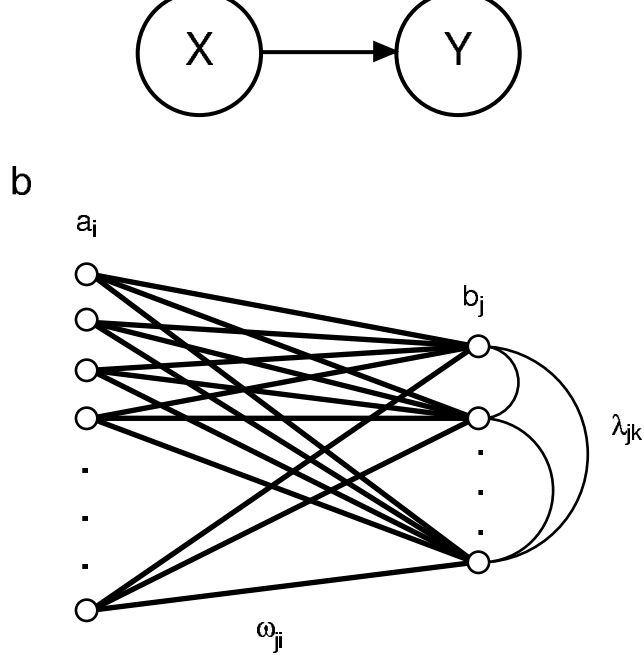


Figure 8: Conversion of a Bayesian belief network into a neural network. (a) Underlying graphical structure for the communication channel. The random variable  $X$  is directly relevant to the random variable  $Y$ . (b) Schematic drawing of the resulting neural belief network. Feedforward connections  $\omega_{ji}$  drive the neural activities  $b_j$  in a fashion consistent with probabilistic inference, but lateral connections  $\lambda_{jk}$  act as an attractor network, attempting to maintain a stable encoded PDF.

The second type of support is retrospective, or diagnostic, support. This is information propagating opposite to the directions of the graph links, from effect to cause, or, equivalently, from evidence to hypothesis (Pearl, 1988). By specifying  $\rho(y; t)$  instead of  $\rho(x; t)$ , the  $X \rightarrow Y$  inference network features only retrospective support.

Using the same underlying space representation (equations 88 and 89) that we used for the predictive network, we determine the update rule for the retrospective network. We find

$$\frac{dA_\mu(t)}{dt} = K_y \left( \sum_\beta B_\beta(t) \Omega_{\beta\mu} - \sum_\alpha A_\alpha(t) \Upsilon_{\alpha\mu} \right) \quad (97)$$

with feedback weights

$$\Omega_{\beta\mu} = \iint \Psi_\beta(y) \rho(y|x) \Phi_\mu(x) dx dy \quad (98)$$

and lateral weights

$$\Upsilon_{\alpha\mu} = \int \left( \int \rho(y|x) \Phi_\alpha(x) dx \right) \left( \int \rho(y|x) \Phi_\mu(x) dx \right) dy \quad (99)$$

While the feedback weights are identical to the feedforward weights in the predictive network (equation 70), note that the summation in equation 97 is over the first index rather than the second. The lateral

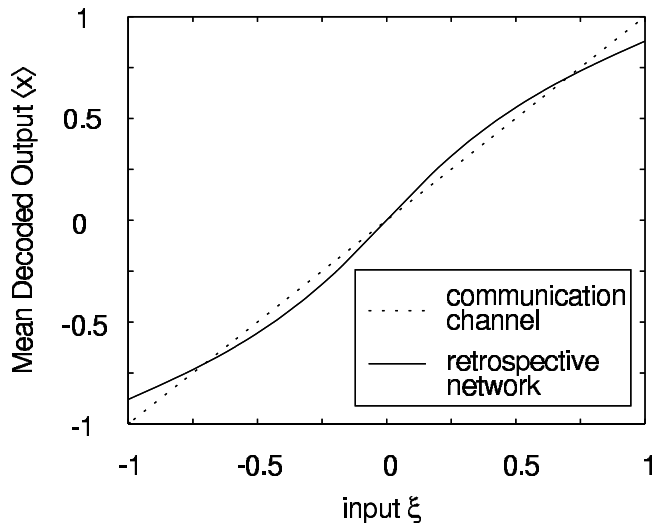


Figure 9: Transfer function for a communication channel implemented in a retrospective neural belief network with 20 neurons for  $X$  and 16 neurons for  $Y$ . The feedback connections yield a transfer function very similar to that produced by the feedforward connections in a predictive network (Figure 6).

weights provide a measure of the correlation between what the different basis functions in the parent node  $X$  predict about the child node  $Y$ ; these lateral connections act to ensure consistency between evidence and hypothesis.

Although it functions differently from the network driven by predictive support, the network driven by retrospective support is capable of capturing identical relations. For example, we can set  $\rho(y|x) = \delta(y-x)$  and produce a retrospective version of the communication channel. We convert this underlying space network to a neural network with piecewise linear activities and an underlying space with two linear basis functions. Despite the different network connectivity, the retrospective network performs comparably to the predictive network, as measured by the transfer functions for the expectation values (Figure 9) of stable states of the neural belief networks.

## 5 Applications of Neural Belief Networks

### 5.1 Bidirectional Propagation

So far, we have restricted our attention to developing neural networks that encode simple probabilistic models involving only one or two random variables. Given suitable representations (Barber, 1999), we can design neural networks that capture a wide variety of probabilistic relations. Further, by regarding representations of probabilistic dependence models as Bayesian belief networks, we have seen that two types of information propagation come into play: predictive and retrospective.

In this section, we will examine several applications of neural belief networks. Unlike those considered before, the probabilistic models will now feature multiple sources of evidence, with bidirectional propagation of both predictive and retrospective support. The corresponding

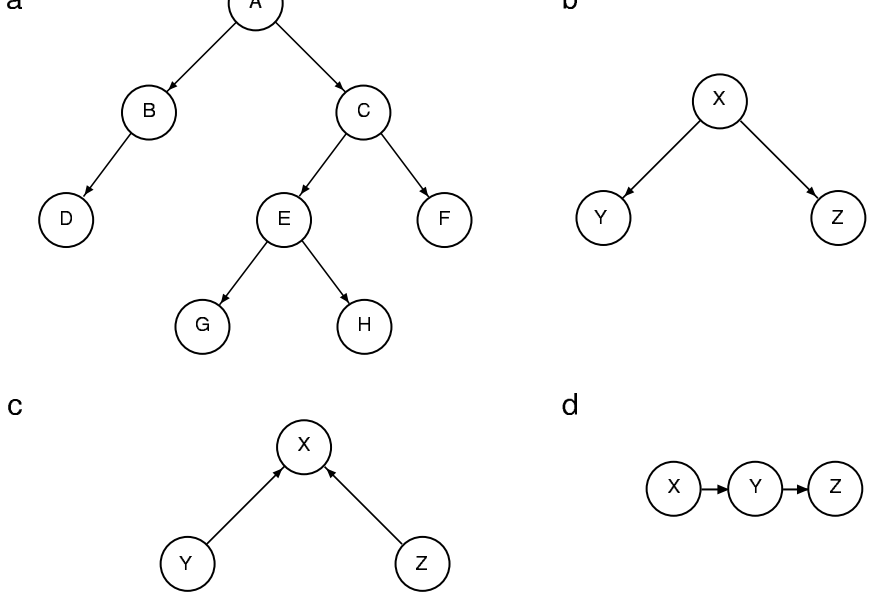


Figure 10: Tree-structured Bayesian belief networks. (a) In this tree, node  $A$  is called the root, while nodes  $D$ ,  $F$ ,  $G$ , and  $H$  are called the leaves. For trees, the direct parent of a node is called its father, and its direct children are called its sons. Since each father has at most two sons, the tree shown here is a binary tree. (b) A small tree. Any of the nodes in this tree can be specified as evidence. The two leaf nodes could also provide evidence: both leaves can provide information to the root, but if the root and one of the leaves is specified, the other leaf will only be driven by the root (its Markov blanket). (c) A tree-like graph with the arrows reversed. Any two of the nodes can be specified and its information will propagate throughout the network. Unlike the case of the tree, the Markov blanket of any node is both of the other nodes. (d) Chains are special cases of trees. This three-node chain can feature both predictive and retrospective support.

neural networks thus have neurons with both feedforward and feedback connections, as well as lateral connections.

## 5.2 Neural Propagation of Evidence in Trees

To facilitate investigation of information propagation in neural belief networks, we first focus on networks whose implicit spaces are specified by tree-structured Bayesian belief networks (Figure 10a). These implicit networks are general enough to illustrate the concepts, but yield neural networks that are readily understood. We will examine binary trees, where each node has at most two children, but the results extend simply to more general tree structures.

We may assume that evidence is only available in the root node and the leaf nodes (although all such nodes need not provide evidence). We may assume that evidence is only available in the root node and the leaf nodes. The root node is the single node which has no father and is located at the top of the tree, while the leaf nodes are all the nodes which have no children. It is not necessary that all such nodes provide evidence. If another node  $X$  was externally specified, the subtree

rooted at  $X$  could be broken off and treated separately. Conversely, the father node of  $X$  is unaffected by the descendants of  $X$ , so they may be deleted from the original tree, leaving  $X$  as a leaf node.

Clearly, an unspecified root node can only receive retrospective support, while an unspecified leaf node can only receive predictive support. All other unspecified nodes in the tree will receive both retrospective and predictive support. We will thus need to consider separately these three types of nodes when determining the update rules for the neural network.

An unspecified root node  $X$  with children  $Y$  and  $Z$  receives feedback inputs (retrospective support) from both of them. We introduce the representations

$$\rho(x; t) = \sum_{\alpha} A_{\alpha}(t) \Phi_{\alpha}(x) \quad (100)$$

$$\rho(y; t) = \sum_{\beta} B_{\beta}(t) \Psi_{\beta}(y) \quad (101)$$

$$\rho(z; t) = \sum_{\gamma} C_{\gamma}(t) \Theta_{\gamma}(z) \quad (102)$$

Following the procedures described in section 4.2, the update rule for the root is

$$\frac{dA_{\mu}}{dt} = -\beta_y \frac{\partial E_y}{\partial A_{\mu}} - \beta_z \frac{\partial E_z}{\partial A_{\mu}} \quad (103)$$

with

$$\begin{aligned} \frac{\partial E_y}{\partial A_{\mu}} = & \sum_{\alpha} A_{\alpha}(t) \int \left( \int \rho(y|x) \Phi_{\alpha}(x) dx \right) \left( \int \rho(y|x) \Phi_{\mu}(x) dx \right) dy \\ & - \sum_{\beta} B_{\beta}(t) \iint \Psi_{\beta}(y) \rho(y|x) \Phi_{\mu}(x) dx dy \end{aligned} \quad (104)$$

and

$$\begin{aligned} \frac{\partial E_z}{\partial A_{\mu}} = & \sum_{\alpha} A_{\alpha}(t) \int \left( \int \rho(z|x) \Phi_{\alpha}(x) dx \right) \left( \int \rho(z|x) \Phi_{\mu}(x) dx \right) dz \\ & - \sum_{\gamma} C_{\gamma}(t) \iint \Theta_{\gamma}(z) \rho(z|x) \Phi_{\mu}(x) dx dz \end{aligned} \quad (105)$$

Thus, the firing rates for the root node are driven by a sum of feedback inputs that individually are identical to the input produced by a single source of retrospective support (section 4.4). The temperature parameters  $\beta_y$  and  $\beta_z$  need not be identical; different values may be used to give greater significance to one of the inputs.

The firing rates for an unspecified leaf node are also updated by a familiar rule. Consider a leaf node  $X$  with father  $U$ . Using the representations

$$\rho(x; t) = \sum_{\alpha} A_{\alpha}(t) \Phi_{\alpha}(x) \quad (106)$$

$$\rho(u; t) = \sum_{\delta} D_{\delta}(t) \Lambda_{\delta}(u) \quad (107)$$

we determine the update rule

$$\frac{dA_{\mu}}{dt} = -\beta_x \frac{\partial E_x}{\partial A_{\mu}} \quad (108)$$

where

$$\frac{\partial E_x}{\partial A_{\mu}} = A_{\mu}(t) - \sum_{\delta} D_{\delta}(t) \iint \Lambda_{\delta}(u) \rho(x|u) \Phi_{\mu}(x) du dx \quad (109)$$

This update rule is of course identical to update rule for the  $X \rightarrow Y$  network with predictive support (section 4.3).

All nonroot, nonleaf nodes have similar update rules. For a node  $X$  with father  $U$  and sons  $Y$  and  $Z$ , we impose the representations

$$\rho(x; t) = \sum_{\alpha} A_{\alpha}(t) \Phi_{\alpha}(x) \quad (110)$$

$$\rho(y; t) = \sum_{\beta} B_{\beta}(t) \Psi_{\beta}(y) \quad (111)$$

$$\rho(z; t) = \sum_{\gamma} C_{\gamma}(t) \Theta_{\gamma}(z) \quad (112)$$

$$\rho(u; t) = \sum_{\delta} D_{\delta}(t) \Lambda_{\delta}(u) \quad (113)$$

Applying the procedure of section 4.2 yields an update rule with form

$$\frac{dA_{\mu}}{dt} = -\beta_y \frac{\partial E_y}{\partial A_{\mu}} - \beta_z \frac{\partial E_z}{\partial A_{\mu}} - \beta_x \frac{\partial E_x}{\partial A_{\mu}} \quad (114)$$

The partial derivatives of the cost functions are identical to those evaluated for the root and leaf nodes. The descendants and ancestors of  $X$  thus communicate, in the neural network, only through the intermediary of  $X$  itself. This is consistent with the tree structure of the underlying Bayesian belief network; given  $X$ , the descendants of  $X$  are conditionally independent of the ancestors of  $X$  (Pearl, 1988).

With these update rules, evidence provided at the root node or at leaf nodes will propagate throughout the network. The manner in

which evidence is specified will depend on how the probabilistic model is posed. Therefore, the same graph could have different nodes specified for different purposes. For instance, the small tree in Figure 10b could have any of its nodes represent sensory inputs.

If we specify the PDF for the root node, the leaf nodes  $Y$  and  $Z$  will receive predictive support from  $X$ . By selecting appropriate representations for the PDFs and conditional probabilities for the links, the resulting neural network could subdivide a complex, highly general sensory input into simpler, more specialized components. For example, a visual input at a particular retinal location might be separated into contrast and color.

Conversely, if we specify PDFs for the leaf nodes, the root node  $X$  will receive retrospective support from  $Y$  and  $Z$ . Amongst other possibilities, this provides a simple way to model redundant sensory inputs. If we take the conditional probabilities to be of narrow Gaussian form,  $\rho(y|x) = N(y; x, \sigma_y^2)$  and  $\rho(z|x) = N(z; x, \sigma_z^2)$ , then the firing rates representing  $\rho(x;t)$  will be updated so as to pool the diagnostic information from both the sensory inputs,  $Y$  and  $Z$ .

Similar arguments apply to larger trees. Additionally, larger trees may well have the root node and leaf nodes specified simultaneously (which is not of interest for the small tree discussed above). These nodes may correspond to sensory inputs, or can represent priors that are built into the neural network.

It is important to recognize that the neural update rules developed above apply only with the directions in the graphs pointing from father to son. If the arrows are reversed, rather different neural update rules are produced. For example, the directions of the small tree shown in Figure 10b can be reversed, as shown in Figure 10c. Specifying  $Y$  and  $Z$  yields the multiplicative update rule

$$\begin{aligned} \frac{1}{K_x} \frac{dA_\alpha(t)}{dt} = & -A_\alpha(t) \\ & + \sum_{\beta, \gamma} B_\beta(t) C_\gamma(t) \iiint \Phi_\alpha(x) \rho(x|y, z) \Psi_\beta(y) \Theta_\gamma(z) dx dy dz \end{aligned} \tag{115}$$

while specifying  $X$  and  $Z$  yields

$$\begin{aligned}
\frac{1}{K_x} \frac{dB_\nu(t)}{dt} = & \\
& - \sum_{\beta, \gamma_1, \gamma_2} B_\beta(t) C_{\gamma_1}(t) C_{\gamma_2}(t) \int \left\{ \left( \iint \rho(x|y, z) \Psi_\beta(y) \Theta_{\gamma_1}(z) dy dz \right) \right. \\
& \qquad \qquad \qquad \left. \left( \iint \rho(x|y, z) \Psi_\nu(y) \Theta_{\gamma_1}(z) dy dz \right) \right\} dx \\
& + \sum_{\alpha, \gamma} A_\alpha(t) C_\gamma(t) \iiint \Phi_\alpha(x) \rho(x|y, z) \Psi_\nu(y) \Theta_\gamma(z) dx dy dz
\end{aligned} \tag{116}$$

This latter update rule features a feedforward term that is multilinear in the firing rates  $\{A_\alpha(t)\}$  and  $\{C_\gamma(t)\}$ . It also features a nonlinear lateral combination of the firing rates  $\{B_\beta(t)\}$  and  $\{C_\gamma(t)\}$  which serves to ensure that the two parent nodes  $Y$  and  $Z$  are mutually consistent with the PDF of the child node  $X$ . If only  $X$  is specified, there will be an additional update rule for the firing rates  $\{C_\gamma(t)\}$  that is similar in form to equation 116.

Although the update rules are more complicated with the directions reversed in this manner, the probabilistic model may demand it. For instance, the Bayesian belief network in Figure 10c is appropriate for implementing the arithmetic operations (add, subtract, multiply, and divide).

An interesting and biologically relevant application of these two types of neural belief networks (tree and reversed-tree) is the estimation of the velocity of a moving object. A small tree (Figure 10b) can generate two copies  $Y$  and  $Z$  of the input position  $X$  by taking the conditional probabilities to be Dirac delta functions  $\delta(y - x)$  and  $\delta(z - x)$ . Due to the attractor-like properties of neural belief nets, we can choose the temperature parameters so that the values of the copies will be held for different lengths of time (see section 4.3). In particular, we can establish the relations

$$\rho(y; t) = \rho(x; t - \tau) \tag{117}$$

$$\rho(z; t) = \rho(x; t - 2\tau) \tag{118}$$

These copies of the position can then be used as the inputs to a Bayesian belief network of the type shown in Figure 10c. By setting  $\rho(v|y, z) = \delta(v - (y - z)/\tau)$ , the velocity at time  $t - \tau$  (Figure 11) can be estimated.

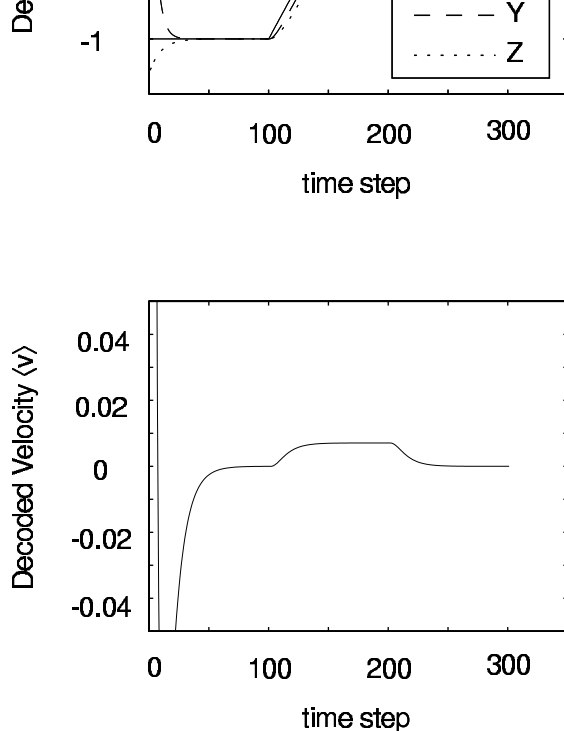


Figure 11: A neural belief network can estimate the velocity of a moving target. (a) The position of the target is copied into two different populations of neurons, with different time delays. (b) The time delay and the difference of the two copies of position are used to estimate the velocity. The results shown here were obtained with the PDFs for each of the random variables represented using underlying spaces spanned by two straight-line basis functions (Figure 2a).

### 5.3 Top-Down Feedback From a High-Level Model

In section 5.2, we examined the neural update rules for Bayesian belief networks with tree-structured graphs. By doing so, we examined the means by which information propagates throughout the network from one or more sources. In particular, we saw that conditional independence in the Bayesian belief network was preserved in the neural network.

We now turn from the general rules by which probabilistic information propagates in the neural network and investigate in more detail the effects that multiple sources of evidence have on the encoded PDFs. We consider PDFs encoded by chains of nodes with evidence provided at one or both ends. (Specifying the PDF for any other node breaks the chain into two chains that can be treated independently.) A chain is a special case of a tree, so the neural update rules can be obtained as in section 5.2.

To allow for a variety of PDFs, we employ representations of higher dimensionality than those generally used in the preceding developments. For each graph node, the interval  $[-1, 1]$  is covered with ten Gaussians (Figure 12a), from which an orthonormal basis is generated. This makes it possible to represent a variety of PDFs, including multimodal distributions.

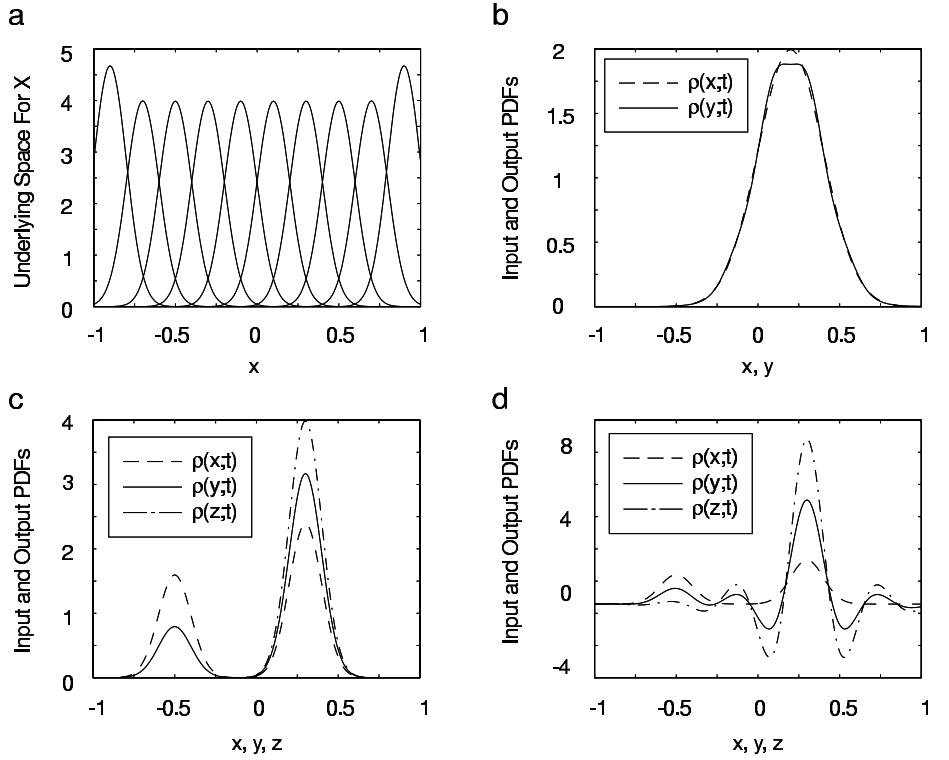


Figure 12: Propagation of evidence in chain-structured neural belief networks. (a) Gaussian functions spanning the underlying spaces for the chain-structured neural belief networks under consideration. Orthonormal bases for the underlying spaces are formed from these functions. (b) A neural belief network accurately transmits PDFs in a chain of two nodes. The decoded output PDF  $\rho(y;t)$  is very similar to the encoded input PDF  $\rho(x;t)$ . (c) Multiple sources of evidence can help to resolve ambiguous information. Here, the inferior mode of a bimodal, bottom-up input  $\rho(x;t)$  is damped by a more specific top-down signal  $\rho(z;t)$ . (d) A high-level model can be dynamically generated in a neural belief network with a population  $Z$  of winner-take-all neurons. An ambiguous input signal at  $X$  is propagated to the winner-take-all neurons through  $Y$ . The winner-take-all neurons only respond to the stronger mode of the bimodal input, which damps the inferior mode in  $\rho(y;t)$ . The functions  $\rho(y;t)$  and  $\rho(z;t)$  are only approximations to PDFs, since they can take on negative values.

The neural firing rate patterns in the explicit space are also assumed to be of Gaussian form. To eliminate any possibility of negative firing rates, the nonlinear activation function is taken to be rectification.

We have already studied at some length the behavior of chains consisting of two nodes (sections 4.3 and 4.4). These chains are able to transmit probabilistic information from one node of the graph to another, with the accuracy limited by the representations chosen. For the predictive network, a feedforward input  $X$  drives the output  $Y$ .

To keep the focus on the interaction of multiple sources of evidence, we take the conditional probability to be a Dirac delta function,  $\rho(y|x) = \delta(y-x)$ —this is, of course, a version of the communication channel that we have extensively considered, but the goal is now to duplicate the PDF rather than a particular numerical value. The input PDF  $\rho(x;t)$  is copied with great fidelity by the output PDF  $\rho(y;t)$  (Figure 12b).

Every chain with three or more nodes will admit both predictive and retrospective support. The behavior of all such chains is well characterized by a chain with three nodes: the update rule for any node depends only on the neighboring nodes, so a chain with three nodes covers all possibilities (only predictive support, only retrospective support, and both predictive and retrospective support). Therefore, we consider the effect of adding a third node to the chain (Figure 10d). We set  $\rho(z|y) = \delta(z-y)$  along with  $\rho(y|x) = \delta(y-x)$  and use identical temperature parameters  $\beta_y$  and  $\beta_z$ .

The first possibility is just to add the third node without adding any additional evidence to the network. We decode  $\rho(y;t)$  and  $\rho(z;t)$  from neural firing rates determined using update rules derived previously for more general trees. For the same input PDF as above,  $\rho(y;t)$  is unchanged by the addition of the retrospective support from the third node, and the structure of  $\rho(z;t)$  is identical to that of  $\rho(y;t)$ .

Since the same evidence was presented to the network, the addition of a third node did not change the behavior of the original nodes. This is entirely appropriate, given the probabilistic foundations of the neural belief networks. However, it is feasible that, by adjusting the temperature parameters or the PDFs representable by the underlying spaces, there can be a change in the dynamics of neural networks extended in this fashion. For example, adjusting the temperature parameters could produce a slowly varying PDF in  $Z$  that is relatively stable against noise, thus stabilizing a more rapidly varying PDF in  $Y$ .

Another possible role that the third node  $Z$  can play is as an additional source of evidence. We directly specify  $\rho(z;t)$  and encode it into the neural network. The neural firing rates for  $Y$  are driven by predictive support from  $X$  and retrospective support from  $Z$ , and then decoded to find  $\rho(y;t)$ . One possible use of this second source of evidence is to resolve an ambiguous input; the inferior mode of a bimodal

predictive input can be de-emphasized using more specific retrospective evidence (Figure 12c).

Although this use of the retrospective evidence resolves the ambiguous predictive input, it is an unsatisfying solution because it does not explain how the retrospective evidence comes about. Ideally, we would like to build up a high-level model of the predictive input, and use this model to generate a top-down signal that imposes global regularity on the bottom-up predictive input. The probabilistic underpinnings of the neural belief network are actually somewhat of a hindrance for this purpose—probabilities account well for multiple possibilities, but here we want to choose only one of those possibilities.

In principle, we could restrict the allowed PDFs for  $\rho(z; t)$  by imposing a prior on the PDFs and rederiving our neural update rules. However, we will adopt a more direct approach and take the neurons representing  $\rho(z; t)$  to be winner-take-all units. Only one of these neurons will be active at a time; the neurons compete to be active, and the single neuron that is most strongly driven will be the one that is activated. The manner of implementation of the winner-take-all units is immaterial, so we directly choose the most strongly driven neuron in the computer simulations. (It is possible to implement a set of winner-take-all units in a real network through a correct choice of nonlinear activation function and lateral weights. Each neuron must inhibit the others and have a self-excitatory connection. See Hertz *et al.*, 1991.)

Since only the most strongly-driven winner-take-all neuron is activated, this strategy provides us with a way to generate a high-level model that selects the dominant mode of a multimodal input distribution. We allow  $Z$  to be driven by the predictive support from  $Y$ , and the winner-take-all nature of the  $Z$  neurons permits only narrow Gaussian PDFs to be represented. Thus,  $\rho(z; t)$  serves as our high-level model, and can resolve ambiguous inputs, as demonstrated in Figure 12d. This type of neural network could be used as the starting point for models of attentive effects in the primate visual system, the electrosensory system of weakly electric fish, or other neural systems where an internal model is built up to impose global constraints on neural representations of information.

## 6 Conclusions

We have examined some of the consequences of the hypothesis that neural networks represent information as probability density functions. These PDFs are assumed to be obtainable by a linear combination of some implicit decoding functions, with the decoder for each neuron being weighted by its firing rate. The firing rates in turn are obtainable from the PDF using a complementary set of encoding functions.

The encoding and decoding functions that we have introduced define spaces of very high dimension, far beyond the range of accurate representation by biological neurons having a precision of only a few bits. To mediate this conflict between computational requirements and biological reality, we have introduced an auxiliary representation of a lower-dimensional underlying space appropriate to the nature and scale of the computations that neurobiological systems actually perform on the relevant input and output analog variables. The basis functions in this underlying space are used to represent both the encoding and decoding functions, limiting the dimensionality of the spaces they define. As an added benefit, the underlying space—the so-called metaneuron space—can be chosen to have properties that are convenient for theoretical characterization of the neural networks resulting from the PDF hypothesis.

Successfully representing an individual PDF with a population of neurons naturally leads one to inquire whether more complex probabilistic models can be represented. We use graphical representations of probabilistic dependence models, in the form of Pearl’s Bayesian belief networks, to organize and simplify the relations between the random variables in the model. Taking advantage of the organizational tool provided by this graphical scheme, we convert a general Bayesian belief network into a neural network that encapsulates the interdependencies of the probabilistic model.

We thus have several ways to represent probabilistic information. We have the implicit model, depicted as a Bayesian belief network; the representation of the probabilistic model in the underlying space; and the representation of the probabilistic model as a neural network in the explicit space. Further, we have devised rules that permit us to convert one type of representation into another type. This formalization of the representation and processing of information in neurobiological computation therefore suggests a general protocol by which probabilistic models can be embedded in neural networks. First, we specify the probabilistic model, using a Bayesian belief network to organize the random variables. We then consider what sorts of functions are exemplars of the PDFs describing the random variables and use these exemplars to define the underlying space. Finally, we utilize the relations between the underlying space and the explicit space to generate the neural network itself.

Researchers in the fields of molecular biology, immunology, genetics, development, and evolution, all of which involve highly complex systems having many degrees of freedom, are beginning to explore the use of “metavariables” as a formal means to reduce the dimensionality of the space of parameters that must be dealt with in achieving viable and tractable quantitative descriptions. The formal results we have derived for metavariable (“metaneuron”) representation of function spaces and

the experience we have gained through associated model simulations may prove valuable for parallel investigations in these and other fields.

## Acknowledgements

This research was supported by the National Science Foundation under Grant Nos. IBN-9634314, PHY-9602127, and PHY-9900713. While writing this work, MJB was a member of the Graduiertenkolleg Azen-trische Kristalle, GK549 of the DFG; the writing was completed while MJB and JWC were participants in the Research Year on “The Sci-ences of Complexity: From Mathematics to Technology to a Sustain-able World” at the Zentrum für interdisziplinäre Forschung, University of Bielefeld.

## References

- [Abbott and Dayan, 1999] Abbott, L. and Dayan, P. (1999). The ef-fect of correlated variability on the accuracy of a population code. *Neural Comput.*, 11(1).
- [Abbott and Kepler, 1990] Abbott, L. and Kepler, T. (1990). Model neurons: From Hodgkin-Huxley to Hopfield. In Garrido, L., edi-tor, *Statistical Mechanics of Neural Networks*, pages 5–18, Berlin. Springer-Verlag.
- [Anderson, 1994] Anderson, C. (1994). Basic elements of biological computational systems. In Potvin, J., editor, *Proceedings of the 2nd IMACS Conference on Computational Physics*, pages 135–137, Singapore. World Scientific.
- [Anderson and Abrahams, 1987] Anderson, C. and Abrahams, E. (1987). The Bayes connection. In *Proceedings of the IEEE First In-ternational Conference on Neural Networks*, volume III, pages 105–112, San Diego, CA. IEEE, SOS Print.
- [Anderson and Van Essen, 1987] Anderson, C. and Van Essen, D. (1987). Shifter circuits: a computational strategy for directed visual attention and other dynamic neural processes. *Proc. Natl. Acad. Sci. USA*, 84(17):6297–6301.
- [Barber, 1999] Barber, M. (1999). *Studies in Neural Networks: Neural Belief Networks and Synapse Elimination*. PhD thesis, Washington University, Saint Louis, MO.
- [Bialek and Rieke, 1992] Bialek, W. and Rieke, F. (1992). Reliability and information transmission in spiking neurons. *Trends Neurosci.*, 15(11):428–434.

- [Bialek et al., 1991] Bialek, W., Rieke, F., de Ruyter van Steveninck, R., and Warland, D. (1991). Reading a neural code. *Science*, 252(5014):1854–1857.
- [Cash and Yuste, 1998] Cash, S. and Yuste, R. (1998). Input summation by cultured pyramidal neurons in linear and position-independent. *J. Neurosci.*, 18(1):10–15.
- [Dayan and Hinton, 1996] Dayan, P. and Hinton, G. (1996). Varieties of Helmholtz machines. *Neural Networks*, 26:1385–1403.
- [Eliasmith and Anderson, 1999] Eliasmith, C. and Anderson, C. (1999). Developing and applying a toolkit from a general neurocomputational framework. *Neurocomputing*, 26:1013–1018.
- [Fuchs et al., 1988] Fuchs, A., Scudder, C., and Kaneko, C. (1988). Discharge patterns and recruitment order of identified motoneurons and internuclear neurons in the monkey abducens nucleus. *J Neurophysiol.*, 60(6):1874–95.
- [Georgopoulos et al., 1986] Georgopoulos, A., Schwartz, A., and Kettner, R. (1986). Neuronal population coding of movement direction. *Science*, 233(4771):1416–19.
- [Hakimian et al., 1999] Hakimian, S., Anderson, C., and Thach, W. (1999). A PDF model of populations of Purkinje cells. *Neurocomputing*, 26:169–75.
- [Haykin, 1999] Haykin, S. (1999). *Neural Networks: A Comprehensive Foundation*. Prentice Hall, Upper Saddle River, NJ, second edition.
- [Hertz et al., 1991] Hertz, J., Krogh, A., and Palmer, R. (1991). *Introduction to the Theory of Neural Computation*. Addison-Wesley Publishing Company, Reading, MA.
- [Hinton and Sejnowski, 1986] Hinton, G. and Sejnowski, T. (1986). Learning and relearning in Boltzmann machines. In Rumelhart, D., McClelland, J., et al., editors, *Parallel Distributed Processing: Explorations in Microstructure of Cognition*, pages 282–317. MIT Press, Cambridge, MA.
- [Mel, 1994] Mel, B. (1994). Information processing in dendritic trees. *Neural Comput.*, 6:1031–85.
- [Neal, 1992] Neal, R. (1992). Connectionist learning of belief networks. *Artificial Intelligence*, 56:71–113.
- [Olshausen et al., 1993] Olshausen, B., Anderson, C., and Van Essen, D. (1993). A neurobiological model of visual attention and invariant pattern recognition based on dynamic routing of information. *J. Neurosci.*, 13(11):4700–19.
- [Olshausen et al., 1995] Olshausen, B., Anderson, C., and Van Essen, D. (1995). A multiscale dynamic routing circuit for forming size-

- and position-invariant object representations. *J. Comput. Neurosci.*, 2(1):45–62.
- [Pearl, 1988] Pearl, J. (1988). *Probabilistic Reasoning in Intelligent Systems: Networks of Plausible Inference*. Morgan Kaufmann Publishers, Inc., San Mateo, CA.
- [Rieke et al., 1997] Rieke, F., Warland, D., de Ruyter van Steveninck, R., and Bialek, W. (1997). *Spikes: Exploring the Neural Code*. MIT Press, Cambridge, MA.
- [Salinas and Abbott, 1994] Salinas, E. and Abbott, L. (1994). Vector reconstruction from firing rates. *J. Comput. Neurosci.*, 1(1–2):89–107.
- [Schwartz, 1993] Schwartz, A. (1993). Motor cortical activity during drawing movements: Population representation during sinusoid tracing. *J. Neurophysiol.*, 70(1):28–36.
- [Seung, 1996] Seung, H. (1996). How the brain keeps the eyes still. *Proc. Natl. Acad. Sci. USA*, 93(23):13339–44.
- [Smyth et al., 1997] Smyth, P., Heckerman, D., and Jordan, M. (1997). Probabilistic independence networks for hidden Markov probability models. *Neural Comput.*, 9:227–69.
- [Theunissen et al., 1996] Theunissen, F., Roddey, J., Stufflebeam, S., Clague, H., and Miller, J. (1996). Information theoretic analysis of dynamical encoding by four identified primary sensory interneurons in the cricket cercal system. *J. Neurophysiol.*, 75(4):1345–64.
- [Van Essen et al., 1992] Van Essen, D., Anderson, C., and Felleman, D. (1992). Information processing in the primate visual system: an integrated systems perspective. *Science*, 255(5043):419–23.
- [Yang and Zemel, 2000] Yang, Z. and Zemel, R. (2000). Managing uncertainty in cue combination. In Solla, S., Leen, T., and Müller, K., editors, *Advances in Neural Information Processing Systems 12*, Cambridge, MA. MIT Press.
- [Zemel, 1999] Zemel, R. (1999). Cortical belief networks. In Hecht-Nielsen, R., editor, *Theories of Cortical Processing*. Springer-Verlag, Berlin.
- [Zemel and Dayan, 1999] Zemel, R. and Dayan, P. (1999). Distributional population codes and multiple motion models. In Kearns, M., Solla, S., and Cohn, D., editors, *Advances in Neural Information Processing Systems 11*, Cambridge, MA. MIT Press.
- [Zemel et al., 1998] Zemel, R., Dayan, P., and Pouget, A. (1998). Probabilistic interpretation of population codes. *Neural Comput.*, 10(2):403–30.